

# Journal of Materials Chemistry A

Accepted Manuscript



This is an *Accepted Manuscript*, which has been through the Royal Society of Chemistry peer review process and has been accepted for publication.

*Accepted Manuscripts* are published online shortly after acceptance, before technical editing, formatting and proof reading. Using this free service, authors can make their results available to the community, in citable form, before we publish the edited article. We will replace this *Accepted Manuscript* with the edited and formatted *Advance Article* as soon as it is available.

You can find more information about *Accepted Manuscripts* in the [Information for Authors](#).

Please note that technical editing may introduce minor changes to the text and/or graphics, which may alter content. The journal's standard [Terms & Conditions](#) and the [Ethical guidelines](#) still apply. In no event shall the Royal Society of Chemistry be held responsible for any errors or omissions in this *Accepted Manuscript* or any consequences arising from the use of any information it contains.

## A facile one-step synthesis of three-dimensionally ordered macroporous N doped TiO<sub>2</sub> with ethanediamine as the nitrogen source

Cite this: DOI: 10.1039/x0xx00000x

Received 00th xxxxxx 201x,  
Accepted 00th xxxxxx 201x

DOI: 10.1039/x0xx00000x

www.rsc.org/

Ting Wang,<sup>a</sup> Xiaoqing Yan,<sup>a</sup> Shishun Zhao,<sup>a</sup> Bo Lin,<sup>a</sup> Chao Xue,<sup>a</sup> Guidong Yang,<sup>\*a</sup> Shujiang Ding,<sup>b</sup> Bolun Yang,<sup>a</sup> Chuansheng Ma,<sup>c</sup> Guang Yang<sup>c</sup> and Guorui Yang,<sup>d</sup>

In this paper, three-dimensionally ordered macroporous (3DOM) N doped anatase TiO<sub>2</sub> (N-TiO<sub>2</sub>) photocatalysts with well-defined macroporous skeletons were prepared using a simple one-step colloidal crystal templating method, and the organic ammonia, ethanediamine, was used as nitrogen source in the preparation to enhance nitrogen incorporation into TiO<sub>2</sub> lattice. The photocatalytic performance of the as-prepared 3DOM N-TiO<sub>2</sub> was investigated by measuring the degradation of rhodamine B (RhB) and the generation of H<sub>2</sub> from water splitting under simulated visible light conditions. In comparison with the pure TiO<sub>2</sub> and N doped TiO<sub>2</sub>, the results of photodegradation and photocatalytic hydrogen generation reactions showed that the 3DOM N-TiO<sub>2</sub> sample had excellent catalytic activity under visible light irradiation. Besides, various analytical techniques have been used to characterize the crystal phase, morphology and optical absorption of the obtained samples. The results showed that 3DOM N-TiO<sub>2</sub> catalyst was successfully synthesized by the one-step colloidal crystal templating method and the as-prepared samples possessed well-defined 3DOM skeleton structure, high crystallinity and enhanced visible-light-driven photocatalytic activities.

### Introduction

It is well known that three-dimensionally ordered macroporous (also called “inverse opals” or “inverted opals”) materials<sup>1</sup> possess uniform pore size, well-defined periodic structure and large surface areas<sup>2,3</sup>, which indicate various potential applications in the fields of battery materials, catalysts or catalysts supporters, sensors, biomaterials<sup>4,5</sup> and photonic crystals<sup>6</sup>, and thus this kind of materials have gained lots of attentions. More recently, a large number of studies have focused on the fabrication of 3DOM materials by a variety of synthetic routs. In particular, the colloidal crystal templating method with polymethyl methacrylate (PMMA), monodisperse silica, or polystyrene (PS) spheres as template agent has received significant attentions because of its low cost and high repeatability<sup>1</sup>. To date, some advances in preparing 3DOM-structured materials (e.g., 3DOM-structured C<sup>7</sup>, MnO<sub>2</sub><sup>8</sup>, Mn<sub>2</sub>O<sub>3</sub>, Fe<sub>2</sub>O<sub>3</sub>, Co<sub>3</sub>O<sub>4</sub>, NiO, CuO<sup>9</sup>, PbO<sub>2</sub><sup>10</sup>) have been achieved.

As a class of important semiconductor materials, porous TiO<sub>2</sub> catalysts have drawn more and more interests due to its special optoelectronic and physiochemical properties, especially for the TiO<sub>2</sub> with 3DOM structure, which has been became a hotspot in the field of porous materials owing to its several great merits for photocatalysis, such as ordered and

uniform macroporous structure, larger surface area, better mass transfer properties and higher light absorption efficiency caused by the multiple scattering and slow photons<sup>11</sup>, and these mentioned-above advantages could efficiently lead to the enhancement of photocatalytic activity of 3DOM TiO<sub>2</sub><sup>12</sup>. However, the relatively broad band gap of 3DOM anatase titania (3.2 eV) and the rapid recombination of photogenerated electron-hole pairs, all of which further limit its large-scale applications<sup>13,14</sup>. In order to overcome the drawbacks and improve the photocatalytic activity, lots of efforts to explore various strategies (e.g. doping with anion<sup>15-17</sup>, combing with narrow band gap semiconductor<sup>18-20</sup>) to modify the TiO<sub>2</sub> photocatalyst have been made. Among these strategies, the nonmetal doping has been frequently applied for achieving visible-light-active TiO<sub>2</sub> photocatalyst, particular TiO<sub>2</sub> with nitrogen doping, which have been extensively investigated over the past decades because such doping not only could effectively modify TiO<sub>2</sub> energy band gap and accelerate the electron-hole separation but also could lead to an apparent red-shift in the optical absorption edge of TiO<sub>2</sub> to lower energy, consequently resulting in the significant improvement of photocatalytic activity under visible light. Until now, a variety of nitrogen sources, such as urea<sup>21</sup>, guanidine carbonate<sup>22</sup>, ammonium hydroxide<sup>23</sup> and ethanediamine<sup>24</sup>, etc, have been explored to

synthesize TiO<sub>2</sub> nanocrystal with N doping. Among these nitrogen precursors, ethanediamine, a special organic nitrogen source, was considered as an amazing nitrogen contained species to prepare the N doped TiO<sub>2</sub> photocatalyst, because ethanediamine can be easily dissolved in water or ethylalcohol, and therefore the nitrogen species can be uniformly and effectually introduced into the anatase TiO<sub>2</sub> crystalline structure. So far, very little work has been reported on the preparation of 3DOM TiO<sub>2</sub> materials with N doping, moreover, the complicated preparation process (at least need two or three steps) further limits the exploitation of N doped TiO<sub>2</sub> with 3DOM structure.

In this paper, a simple yet efficient one step colloidal crystal template method was developed to synthesize N doped TiO<sub>2</sub> with three-dimensionally ordered macroporous structure. Meanwhile, using the organic ammonia, ethanediamine, as nitrogen source to achieve the N doping. The as-prepared photocatalysts are characterized by X-ray powder diffraction (XRD), Scanning electron microscopy (SEM), Energy dispersive X-ray spectrometry (EDX), Transmission electron microscopy (TEM), Fourier transform infrared (FT-IR), UV-vis diffuse reflectance spectroscopy (DRS), N<sub>2</sub> adsorption-desorption, and X-Ray photoelectron spectroscopy (XPS). The photocatalytic activity of the 3DOM N-TiO<sub>2</sub> was evaluated by the photodegradation of rhodamine B (RhB) and photocatalytic H<sub>2</sub> evolution from water splitting under visible light, which show significantly higher photocatalytic efficiency than the pure N-TiO<sub>2</sub> and TiO<sub>2</sub> nanoparticles.

## Experimental

### Synthesis of 3DOM N doped TiO<sub>2</sub>

PMMA spheres were prepared by modified emulsifier-free emulsion polymerization of MMA, as described elsewhere<sup>25</sup>. 3DOM N-TiO<sub>2</sub> catalysts were synthesized through one step colloidal crystal templating method. Briefly, 0.01 mol of tetrabutyl titanate was dissolved into 30 mL of ethanol solution containing 1 mL of glacial acetic acid under vigorous stirring to form solution of TiO<sub>2</sub> precursor, and 0.01 mol of ethanediamine was added to the above TiO<sub>2</sub> precursor solution accompanying with continuously stirring for 30 min at room temperature to form mixture solution. Then 3 g PMMA was immersed into the mixture and kept at room temperature overnight to obtain the monolith of 3DOM N-TiO<sub>2</sub> precursor. Afterwards, the monolith was dried at 80 °C overnight and then calcined at 500 °C for 4 h with a ramp rate of 1 °C/min in muffle furnace under stationary air to obtain the final 3DOM N-TiO<sub>2</sub> catalyst. For comparison, the N-TiO<sub>2</sub> nanoparticles were synthesized by the same process without addition of PMMA template. The pure TiO<sub>2</sub> nanoparticles were also prepared using the mentioned-above method without the addition of ethanediamine and PMMA template.

### Characterizations

The crystalline structure and phase component were obtained on the X-ray powder diffraction (XRD; SHIMADZU, Lab X XRD-6000). The geometry and morphology of the catalyst

were acquired by the field-emission scanning electron microscope (JEOL, JSM-6700F) and the energy dispersive X-ray spectroscopy (EDX) was employed for elemental analysis. The structure and surface state of photocatalyst composites were gained on the transmission electron microscopy (JEOL, JEM-2100). Fourier transform infrared (FT-IR) spectra (Nicolet avatar 360) was used to obtain the information of function groups on the surface of materials by potassium bromide tablet method. The optical properties of the samples were detected using a Hitachi U-4100 UV/Vis spectrometer in diffuse reflectance mode with BaSO<sub>4</sub> as the reflectance. The spectra were recorded at room temperature in the range between 200 nm and 700 nm. N<sub>2</sub> adsorption-desorption isotherms of the samples were collected by an ASAP-3000 BET analyzer to obtain the textural properties of the catalysts. The specific surface area and pore size distribution plots of the as-prepared samples were counted by the Brunauer-Emmett-Teller (BET) equation and Barrett-Joyner-Halenda (BJH) method, respectively. The X-ray photoelectron spectroscopy (XPS) was performed on a Kratos AXIS Ultrabld photoelectron spectrometer with monochromatic Al-K $\alpha$  excitation ( $h\nu=1486.69$  eV) and a charge neutralizer to investigate the elemental contents and electronic states on the surface of the as-prepared samples. The fitted curves were obtained with XPSPEAK software, and all the bonding energies were calibrated to the C (1s) internal standard peak at 284.8 eV.

### Photocatalytic testing

#### Photocatalytic degradation of RhB

The photocatalytic activities of the as-prepared 3DOM N-TiO<sub>2</sub> catalysts were evaluated by decomposing rhodamine B dye under visible-light irradiation at room temperature. An overhead 300 W Xenon lamp (NBET, HSX-F300, Beijing) equipped with UV filter (HSX-UV300) was the simulated photosource and mounted a 420 nm cut-off glass filter in order to ensure only visible light irradiation. The distance between the visible light source and RhB solution is about 10 cm. In each experiment, 0.07 g as-prepared photocatalyst was added into 70 mL aqueous solution of RhB dye (10 mg/L) to perform the reaction suspension. Before the photoreaction, the suspension was magnetically stirred in dark for 40 min to establish an adsorption/desorption equilibrium between the catalyst surface and the RhB solution, after that, the solution was exposed to the visible light with continuously magnetic stirring to carry out the photodegradation reaction. During the photoreaction, about 3 mL the suspension was taken and centrifuged (13000 rpm for 5 min) to remove the catalyst particles every 30 min and the residual RhB was analyzed by UV-vis spectrophotometer (UV-1900PPC, Shanghai, China) at 554 nm to obtain its absorbance values. As is known, the concentration of RhB is directly proportional to its absorbance values. Hence, the degradation efficiency ( $x$ ) of RhB can be calculated by the formulation:  $x=C/C_0\times 100\%$ , where  $C_0$  is the concentration of original RhB solution after 40 min adsorption,

$C$  is the concentration of RhB solution after every 30 min reaction. In addition, the photoactivity of the as-prepared samples under full sunlight irradiation was evaluated by the same process described above except for the Xenon lamp mounted a 420 nm cut-off glass filter.

In order to test the stability and reusability of the as-prepared samples, we did the repeated photocatalytic experiment: 0.07 g 3DOM N-TiO<sub>2</sub> was dispersed in 70 mL RhB solution (10 mg/L), and the procedures of photoreaction were the same as the above description except the photoreaction time, which was limited to 120 min. After each round of the reaction, the mixture was centrifuged to collect the catalysts. Then, the separated catalyst was washed and dried for several hours at 80 °C. Afterwards, the dried samples was added back into the catalytic reaction system to perform the degradation RhB under the same conditions.

### Photocatalytic H<sub>2</sub> evolution from water splitting

The photocatalytic activities of the as-prepared 3DOM N-TiO<sub>2</sub>, N-TiO<sub>2</sub> and TiO<sub>2</sub> nanoparticles were also tested by photocatalytic H<sub>2</sub> evolution under visible light irradiation. The reaction steps as follows: 0.05 g as-prepared catalyst was dispersed in a 50 mL aqueous solution consisted of 0.25 M Na<sub>2</sub>S and 0.35 M Na<sub>2</sub>SO<sub>3</sub> which were used as the sacrificial agents to avoid catalysts photocorrosion. Prior to illumination, the system was bubbled with nitrogen for 15 min to ensure the reaction system is under anaerobic conditions. The amount of H<sub>2</sub> generation was determined on a gas chromatography (Agilent technologies: 6890N) with Thermal Conductivity Detector (TCD) mounted with a 5 Å molecular sieve using N<sub>2</sub> as the carrier gas.

### Results and discussion

3DOM N doped TiO<sub>2</sub> photocatalysts were prepared by one step colloidal crystal templating method, which was considered as one of promising approaches for the fabrication of various kinds of porous materials. The probable synthesis process was schematically illustrated in Fig. 1. As shown, monodisperse PMMA spheres were firstly synthesized by modified emulsifier-free-polymerization method<sup>25</sup>, meanwhile, these monodisperse PMMA spheres can easily self-assemble to form orderly colloidal crystal layer under centrifugal condition. Next, the formation of PMMA colloidal crystal template was immersed into the precursor solution consisting of tetrabutyl titanate (Ti(OBu)<sub>4</sub>) and ethanediamine (C<sub>2</sub>H<sub>4</sub>N<sub>2</sub>H<sub>4</sub>), which were used as titanium source and nitrogen source, respectively. In the initial stages of chemical reaction, the molecules of tetrabutyl titanate rapidly react with ethanediamine to generate the substituted Ti(OBu)<sub>4-n</sub>(C<sub>2</sub>H<sub>4</sub>N<sub>2</sub>H<sub>4</sub>)<sub>n</sub> precursor. With the increase of aging time, countless Ti(OBu)<sub>4-n</sub>(C<sub>2</sub>H<sub>4</sub>N<sub>2</sub>H<sub>4</sub>)<sub>n</sub> micelle was filled into the interstices of PMMA blocks and gradually connected by hydrogen bonding to create an “inverse-opal” structure in three dimensions. The post-treatment of calcinations was followed to obtain the final 3DOM N doped

TiO<sub>2</sub> photocatalysts (a multi-layer porous structure can be clearly seen from the SEM image); this process can effectively remove the PMMA colloidal crystal template and make the nitrogen elements completely incorporate into the lattice of TiO<sub>2</sub>. Simultaneously, the calcinations process also leads to the enhancement of the crystalline degree of N doped TiO<sub>2</sub>, resulting in the higher visible-light-driven photocatalytic activity. It was worthy noted that the structure of the PMMA template and the immersion process were the key factors to get the final N doped TiO<sub>2</sub> with 3DOM structure. If the structure of the PMMA template was unordered or the immersion process was not enough, the structure of the final product was not uniform or ordered.

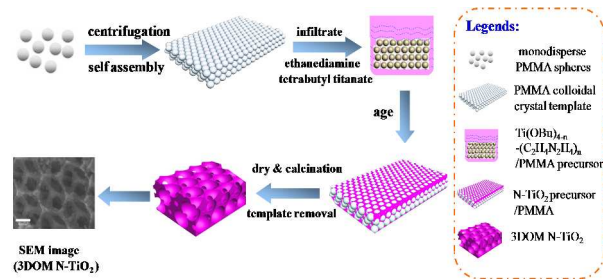


Fig. 1 The schematic synthesis process steps of 3DOM N-TiO<sub>2</sub> sample.

Fig. 2 shows the XRD pattern of 3DOM N-TiO<sub>2</sub>, including TiO<sub>2</sub> and N-TiO<sub>2</sub> nanoparticles data, used as the references. It can be seen that several narrow and sharp peaks located at 2θ values of 25.32°, 37.80°, 48.20°, 53.97°, 55.06°, 62.75°, 68.91°, 70.29°, and 75.07° can be observed in the patterns of all the as-prepared samples, which

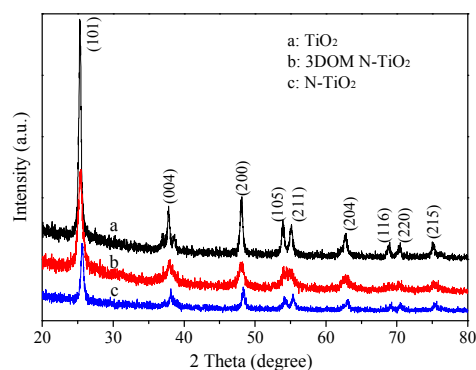


Fig. 2 X-ray diffraction patterns of pure TiO<sub>2</sub>, N-TiO<sub>2</sub> and 3DOM N-TiO<sub>2</sub>.

correspond to the peaks of anatase TiO<sub>2</sub> of (101), (004), (200), (105), (211), (204), (116), (220), and (215) crystal planes (JCPDS: 21-1272), respectively. No other peaks, such as N-O and Ti-N bonds, can be found, indicating that the N element either doped into TiO<sub>2</sub> lattice or highly dispersed on the surface of TiO<sub>2</sub>, which accords with other nitrogen doped TiO<sub>2</sub> reported previously<sup>24,26,27</sup>. In addition, the higher intensity of the main (101) bragg peak anatase show that these samples possess high crystalline structure.

Fig. 3 shows the SEM images of the self-made PMMA template and the as-prepared 3DOM N-TiO<sub>2</sub> sample, including data for N-TiO<sub>2</sub> and TiO<sub>2</sub> nanoparticles, which used here as the references. It can be seen from Fig.3a and b that the N-TiO<sub>2</sub> and pure TiO<sub>2</sub> samples present aggregates structure, which are composed of a large quantity of nanoparticles. Fig.3c clearly

shows that the colloidal crystal template contains a large number of highly ordered close-packed spheres. Meanwhile, the inset of Fig. 3c confirms that the template is made from periodic microspheres with 350 nm diameter. Fig. 3d shows the low magnified SEM image of the as-prepared 3DOM N-TiO<sub>2</sub> catalyst. As can be seen that 3DOM N-TiO<sub>2</sub> catalysts display an open interconnected macroporous network, which is the replication of three-dimensional closely-packed PMMA opals. The opal size of the photocatalysts are smaller than the size of original PMMA template particles, which can be attributed to the shrinkage of the windows size during the calcination. However, the well-defined 3DOM framework still can be observed in the sample, indicating good thermal stability of the samples. Fig. 3e shows the high-magnification SEM image of the N-TiO<sub>2</sub> with 3DOM structure, which obviously showed that the as-prepared N-TiO<sub>2</sub> is 3D-interconnected macroporous networks, consisting of periodic spherical voids. It is noteworthy that each large pore is connected with six neighboring spheres and circular windows where the original PMMA spheres contacted with each other. And the origin of the windows was mainly attributed the fact that PMMA spheres touched so close that Ti(OBu)<sub>4-n</sub>(C<sub>2</sub>H<sub>4</sub>N<sub>2</sub>H<sub>4</sub>)<sub>n</sub> precursor solution did not penetrate those regions.

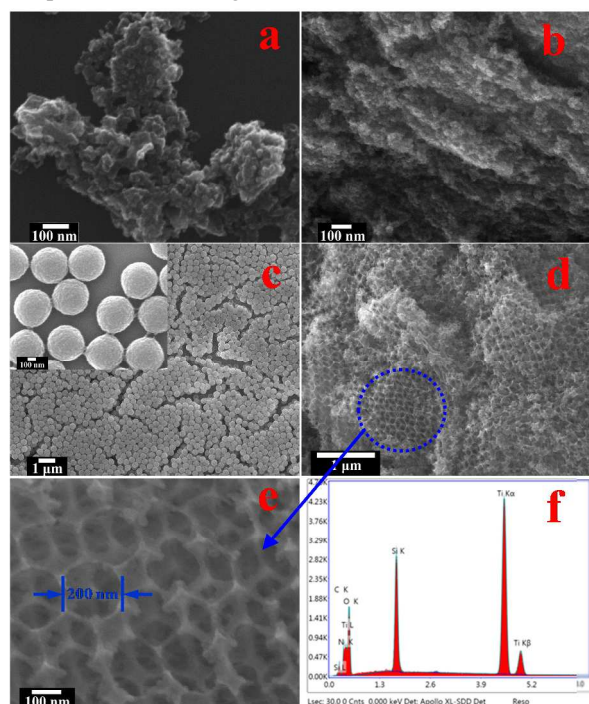


Fig. 3 SEM images of TiO<sub>2</sub> (a); N-TiO<sub>2</sub> (b); PMMA (c); 3DOM N-TiO<sub>2</sub> (d, e); and Energy-dispersive X-ray pattern of 3DOM N-TiO<sub>2</sub> (f).

In addition, Fig. 3f shows the Energy-dispersive X-ray results of the 3DOM N-TiO<sub>2</sub>. The analysis of EDX shows that 3DOM N-TiO<sub>2</sub> catalyst is composed of Ti, O, N, C and Si elements, which confirms the presence of N in the 3DOM N-TiO<sub>2</sub> sample. Carbon (atomic percent of 13.23%) was also observed in the spectra, probably due to the incomplete removal of the PMMA template during calcinations, and the EDX signal

for Si element can be attributed to the utilization of the silicon substrate in SEM testing process.

The typical macroporous structure and crystallization of the 3DOM N-TiO<sub>2</sub> sample were further analyzed by TEM and HRTEM. As shown in Fig. 4a and b, the TiO<sub>2</sub> and N-TiO<sub>2</sub> photocatalysts possess the typical nanoparticle morphology with an average grain size of 15–20 nm, which are in consistence with SEM analysis. The insets of Fig. 4a and b are the selected-area electron diffraction pattern of TiO<sub>2</sub> and N-TiO<sub>2</sub>, which show an obvious bright electron diffraction rings, revealing that the reference samples have good crystallinity, in agreement with XRD analysis. It can be seen from Fig. 4c that the as-obtained 3DOM N-TiO<sub>2</sub> displays well-defined ordered macroporous structure and the formation of porous skeleton of the catalyst are composed of many nanoparticles with size ~10 nm resulting from the aggregation of ultrafine metallic oxide, this is well consistent with the SEM observations. In addition, the presence of the crystal planes and the lattice fringes of the 3DOM N-TiO<sub>2</sub> can be obviously observed in the HR-TEM image (Fig. 4d), which taken on an individual nanoplate of the pore wall. It further proves the good crystallinity of 3DOM N-TiO<sub>2</sub>. The reflections with d spacing values of 0.338 nm observed in Fig. 4b are in good agreement with the TiO<sub>2</sub> crystal (204) lattice planes. Besides, the inset of Fig. 4d shows the selected area electron diffraction (SAED) pattern of 3DOM N-TiO<sub>2</sub>. A sequence of bright electron diffraction rings can be clearly found, which proves the good crystallinity of 3DOM N-TiO<sub>2</sub> in accordance with XRD analysis.

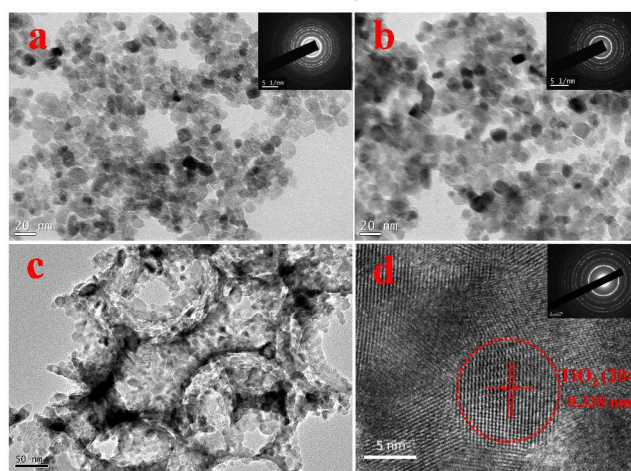


Fig. 4 TEM images of TiO<sub>2</sub> (a); N-TiO<sub>2</sub> (b); 3DOM N-TiO<sub>2</sub> (c); HRTEM image of 3DOM N-TiO<sub>2</sub> (d).

Fig. 5 shows the FT-IR spectra of 3DOM N-TiO<sub>2</sub>, N-TiO<sub>2</sub> and pure TiO<sub>2</sub> nanoparticles, which gives the information of functional groups on the surface of catalyst. All the as-prepared samples present similar FT-IR spectra, and the peak in the range of 400–750 cm<sup>-1</sup> was assigned to the Ti-O stretching and Ti-O-Ti bridging stretching bond. In addition, the absorbance band at 3400 cm<sup>-1</sup> in the three spectra can be attributed to the surface hydroxyl groups and absorbed water molecules<sup>24</sup>. Besides, the FT-IR band at around 1630 cm<sup>-1</sup> in the N doped and pure TiO<sub>2</sub> samples corresponds to the O-H stretching vibration and bending vibration<sup>28,29</sup>, and these absorbed OH

groups and water molecules play a significant role in photocatalytic activity since they act as an oxidizer to decompose organic pollutions<sup>16</sup>.

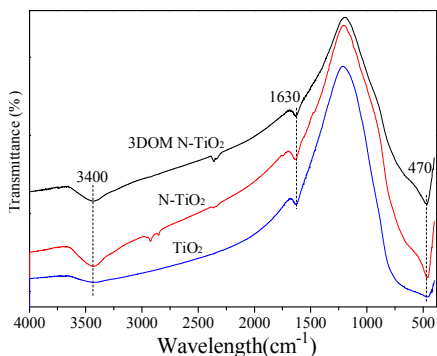


Fig. 5 FT-IR spectra of 3DOM N-TiO<sub>2</sub>, N-TiO<sub>2</sub> and pure TiO<sub>2</sub>.

The nitrogen adsorption-desorption isotherms and BJH pore size distribution curves of 3DOM N-TiO<sub>2</sub>, N-TiO<sub>2</sub> and pure TiO<sub>2</sub> nanoparticles were shown in Fig. 6. It can be seen in Fig. 6(a) the N-TiO<sub>2</sub> and pure TiO<sub>2</sub> nanoparticles exhibit type-IV isotherms according to the IUPAC classification<sup>14</sup>, suggesting that the existence of mesoporous structure in the two samples. It also can be found that an obvious adsorption hysteresis loop at  $0.54 < P/P_0 < 0.99$  was observed in the isotherms of N-TiO<sub>2</sub> and pure TiO<sub>2</sub> samples, which could be classified as type-H3 hysteresis loop, indicating the presence of slit-like pores<sup>13,30</sup>. While, the 3DOM N-TiO<sub>2</sub> exhibits type-II isotherm with a type-H4 hysteresis loops at the high relative pressure ( $P/P_0$ ) range of 0.5-1.0<sup>31</sup>, prominently indicating that the presence of macroporous structure in this materials, which is in agreement with the SEM results.

Table 1 BET surface area, pore volume and pore size of all the prepared photocatalysts.

Catalyst	$S_{\text{BET}}$ m <sup>2</sup> /g	Pore volume (cm <sup>3</sup> /g)	Pore size (nm)
TiO <sub>2</sub>	74.20	0.18	9.90
N-TiO <sub>2</sub>	59.69	0.13	8.89
3DOM N-TiO <sub>2</sub>	50.61	0.35	27.43

Besides, the BET surface area and BJH pore size distribution were determined from the adsorption-desorption isotherm. Table 1 lists the measured surface areas and pore volume of the three photocatalysts. The N-TiO<sub>2</sub> and pure TiO<sub>2</sub> nanoparticles show higher surface area with the value of 59.70 and 74.20 m<sup>2</sup> g<sup>-1</sup>, respectively. Meanwhile, it can be seen from Fig. 6(b) that the pore size distribution calculated by the desorption branch of isotherm for both N-TiO<sub>2</sub> and pure TiO<sub>2</sub> nanoparticles showed similar narrow pore size distribution ranging from 2.32 nm to 7.98 nm, suggesting that the samples possess typical mesoporous structure. In compared with N-TiO<sub>2</sub> and pure TiO<sub>2</sub>, the 3DOM N-TiO<sub>2</sub> sample shows relatively lower surface areas (50.61 m<sup>2</sup> g<sup>-1</sup>), however, the sample exhibits much higher pore volume (0.35 cm<sup>3</sup> g<sup>-1</sup>) than that of N-TiO<sub>2</sub> and pure TiO<sub>2</sub>, this

may be mainly ascribed to the formation of 3D-interconnected macroporous networks in this solid. In addition, it should be noteworthy that the large surface area of the as-prepared catalysts plays an important role in enhancing the photocatalytic activities, yet not a decisive factor<sup>32</sup>, and the formation of 3DOM structure as well as the N doping is the key factors for the enhancement of catalytic performance of 3DOM N-TiO<sub>2</sub>, which will be discussed later.

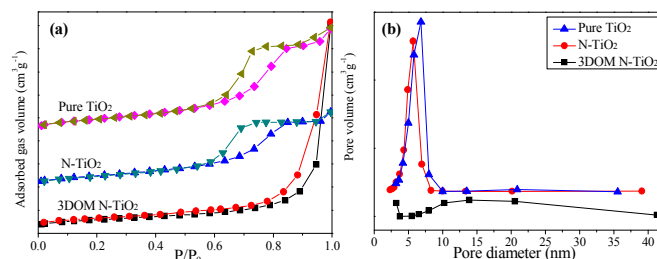


Fig. 6 (a) N<sub>2</sub> adsorption-desorption isotherms of all the samples; (b) corresponding pore size distribution of all the samples.

Fig. 7 shows the UV-vis absorption spectra of 3DOM N-TiO<sub>2</sub>, N-TiO<sub>2</sub> and pure TiO<sub>2</sub> nanoparticles. It can be observed that the pure TiO<sub>2</sub> exhibits photoresponse in the UV region (wavelength below 395 nm) due to its wide energy band gap (3.2 eV). Compared with the pure TiO<sub>2</sub>, TiO<sub>2</sub> sample with N doping show an apparent absorption edge in the visible light region, especially for the 3DOM N-TiO<sub>2</sub> catalyst prepared by one step colloidal crystal templating method, a very broad and flat absorption tail that extends across much of the visible light region down to 650 nm can be observed in the UV-vis absorption spectrum. This phenomenon might be caused by the following two aspects: On the one hand, N species was incorporated into the lattice of TiO<sub>2</sub> and produce a intermediate energy levels, which induced the narrow of TiO<sub>2</sub> band gap and led to a larger and clear red-shift in the optical absorption edge. On the other hand, the architecture structure of the photocatalyst plays a very important role in the enhancement of optical absorption of the N-TiO<sub>2</sub> samples, as well known, three-dimensionally ordered macroporous materials possess the properties of multiple scattering and slow photon effects. Thus, slow photons generated in 3DOM structures have the advantages of increasing the path length of the light, meanwhile, the group velocity of light significantly decreases at the edge of these wavelengths, consequently resulting in the improvement of the visible light harvesting<sup>33</sup>.

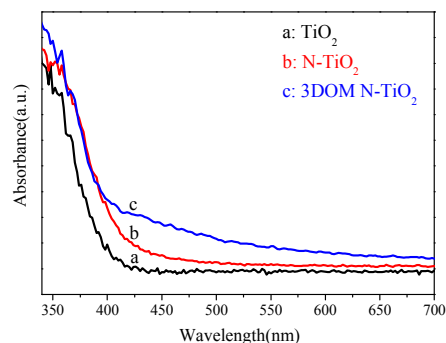


Fig. 7 UV-visible absorption spectra of pure TiO<sub>2</sub>, N-TiO<sub>2</sub> and 3DOM N-TiO<sub>2</sub> samples.

The X-ray photoelectron spectroscopy (XPS) measurements were performed to test the surface chemical components and electronic states of elements on the surface of N doped TiO<sub>2</sub> samples. The whole XPS survey scan spectra show that both of 3DOM N-TiO<sub>2</sub> and N-TiO<sub>2</sub> sample contain N, Ti, O, and C elements, which was in agreement with the EDX analysis and further confirmed the containment of N elements in the samples. Meanwhile, the atomic concentration of N can be calculated based on the XPS data and the values were found to be 0.25 at.% for 3DOM N-TiO<sub>2</sub> and 0.15 at.% for N-TiO<sub>2</sub>, respectively. In addition, the XPS spectra for the C 1s peak might be ascribed to the incomplete removal of the PMMA template during calcination process.

Fig. 8a shows the O 1s XPS spectra of the 3DOM N-TiO<sub>2</sub> and N-TiO<sub>2</sub>. The peak at 529.7 eV is the characteristic of the lattice oxygen of TiO<sub>2</sub>, and the rest of peaks in the range of 531.0~533.3 eV can be assigned to the surface adsorbed components of the hydroxyl group (-OH)<sup>14,16,34</sup>. The Ti 2p XPS spectra of the 3DOM N-TiO<sub>2</sub> and N-TiO<sub>2</sub> nanoparticles are shown in Fig. 8b. Two peaks corresponding to Ti 2p<sub>3/2</sub> and Ti 2p<sub>1/2</sub> were observed at the binding energy of 458.5 and 464.2 eV, respectively, which can be attributed to the characteristic peaks of Ti<sup>4+</sup> on the surface of N-TiO<sub>2</sub> catalysts<sup>35</sup>. There is no Ti<sup>3+</sup> ions observed in the XPS spectra of the two samples. The phenomenon may be due to either the low resolution of the XPS or because the Ti<sup>3+</sup> species exist in the subsurface or bulk.

The N 1s XPS spectra for the two samples are shown in Fig. 8c. The N 1s peak located at 397.6 eV can be assigned to N substituted at oxygen sites (substitutional N) in the TiO<sub>2</sub> crystal lattice to form N-Ti-N bond<sup>36-38</sup>. Besides, in the N 1s XPS spectra of 3DOM N-TiO<sub>2</sub> catalyst, an additional peak at 399.7 eV can be attributed to interstitial N<sup>39,40</sup> atoms in the samples. It is believed that the presence of substitutional N in both of 3DOM N-TiO<sub>2</sub> and N-TiO<sub>2</sub> samples make the main contribution to the visible light absorption and visible-light-induced photocatalytic activity.

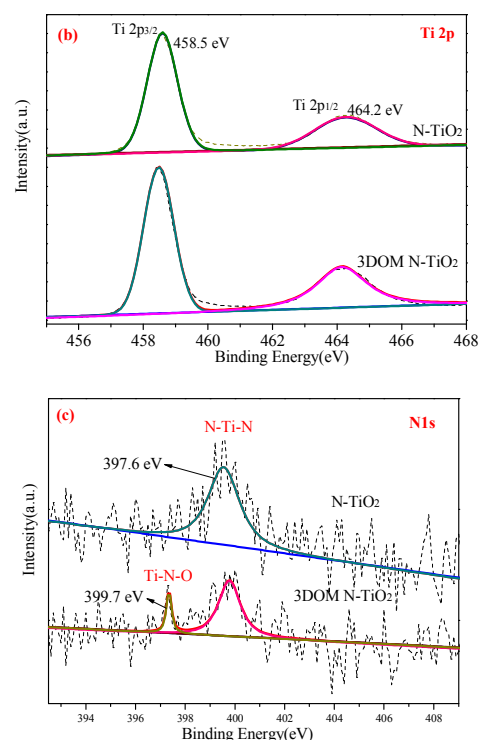
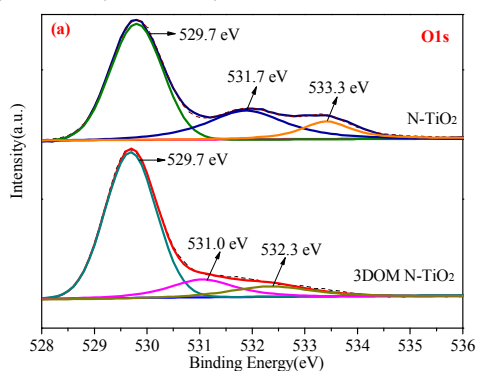


Fig. 8 XPS spectra of N-TiO<sub>2</sub> and 3DOM N-TiO<sub>2</sub> samples. (a) O 1s XPS spectra; (b) Ti 2p XPS spectra; (c) N 1s XPS spectra.

In order to evaluate the photocatalytic performance of the as-prepared catalysts, the generation of hydrogen from water splitting was carried out under visible light irradiation. As illustrated in Fig. 9, the pure TiO<sub>2</sub> nanoparticles show no H<sub>2</sub> evolution within 6 h photoreaction, this is due to the large band gap of TiO<sub>2</sub> and which can not be excited by visible light. While, both the two N-doped samples show significant H<sub>2</sub> generation activity, and the amount of hydrogen produced over N-TiO<sub>2</sub> with 3DOM structure is 122.91 μmol g<sup>-1</sup> under 6 h visible light irradiation, which was higher than that of N-TiO<sub>2</sub> nanoparticles (105.31 μmol g<sup>-1</sup>). Thus, it can be demonstrated that the obtained 3DOM N-TiO<sub>2</sub> by the method mentioned above exhibit excellent properties in photocatalytic hydrogen generation reactions.

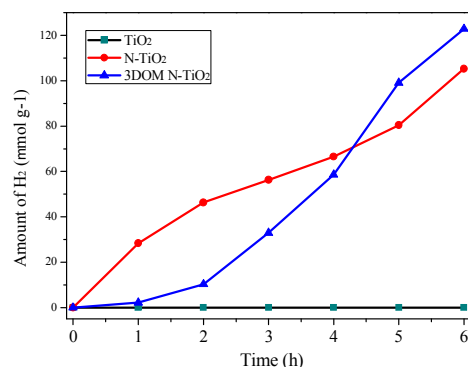


Fig. 9 Photocatalytic H<sub>2</sub> production efficiency over pure TiO<sub>2</sub>, N-TiO<sub>2</sub> and 3DOM N-TiO<sub>2</sub> samples under visible-light irradiation.

In addition to generation H<sub>2</sub> from water splitting, the photocatalytic degradation of the organic pollutants was also evaluated over the as-prepared photocatalysts, and the RhB dye was

chosen as the simulated pollution. Herein, the photocatalytic activities of N-TiO<sub>2</sub> and pure TiO<sub>2</sub> nanoparticles were tested under the same conditions, of which was used as reference. As shown in Fig. 10, no obvious degradation of RhB can be found in the absence of photocatalyst, indicating that the RhB dye is very stable under visible light irradiation. Moreover, the pure TiO<sub>2</sub> nanoparticles show no visible-light-driven activity at all, which can be ascribed to the lower visible light absorption caused by the wide energy band gap of TiO<sub>2</sub><sup>41,42,43</sup>. In contrast, N-TiO<sub>2</sub> nanoparticles and 3DOM N-TiO<sub>2</sub> exhibit stronger photocatalytic performance under visible light irradiation, and the RhB degradation rate is around 76.96% and 87.16%, respectively within 180 min photoreaction. It can be seen that the doping of N element in TiO<sub>2</sub> has a significant effect on the visible-light catalytic activity of titania.

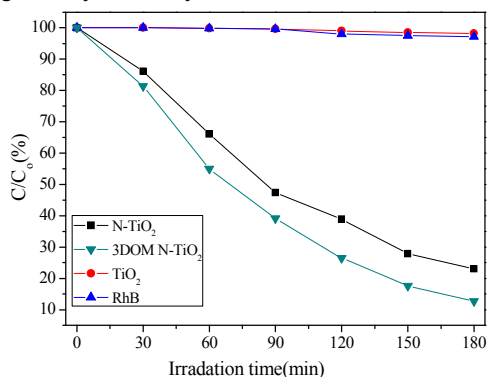


Fig. 10 Photocatalytic degradation of RhB over pure TiO<sub>2</sub>, N-TiO<sub>2</sub> and 3DOM N-TiO<sub>2</sub> samples under visible-light irradiation.

In addition, the photocatalytic degradation of RhB over all the as-prepared samples was evaluated under full sunlight irradiation. As shown in Fig. 11, 3DOM N-TiO<sub>2</sub> and N-TiO<sub>2</sub> nanoparticles showed excellent photocatalytic activities than the pure TiO<sub>2</sub> nanoparticles. After 90 min photodegradation reaction, the degradation rate of RhB solution for 3DOM N-TiO<sub>2</sub>, N-TiO<sub>2</sub> and pure TiO<sub>2</sub> nanoparticles are about 90.41%, 90.86% and 68.25%, respectively, suggesting that doping N atoms into TiO<sub>2</sub> lattice was not only enhanced the visible light activity but also increased the full sunlight photocatalytic performance of samples.

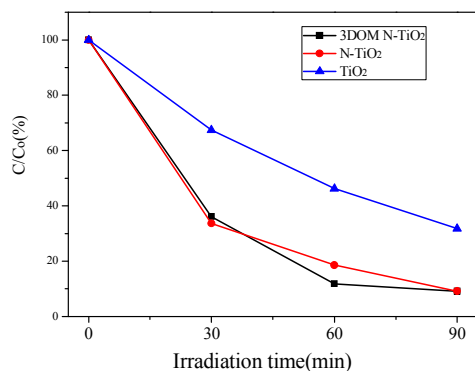


Fig. 11 Photocatalytic degradation of RhB over pure TiO<sub>2</sub>, N-TiO<sub>2</sub> and 3DOM N-TiO<sub>2</sub> samples under full sunlight irradiation.

On basis of above discussion, it can be concluded that 3DOM N-TiO<sub>2</sub> and N-TiO<sub>2</sub> show excellent photoactivities in both photodegradation reactions and H<sub>2</sub> evolution reactions. This

phenomenon can be attributed to the N doping process in our preparation. It is well known that the nitrogen doping can induce the formation of an isolated band above the valence band edge of TiO<sub>2</sub><sup>22,24</sup>, which leads to reduce the energy band gap. Furthermore, the narrowed band gap of 3DOM N-TiO<sub>2</sub> favors the transfer of photogenerated electrons and results in more electrons and holes could participate in the photocatalytic redox reaction. Thus, N-doped TiO<sub>2</sub> exhibit enhanced photocatalytic activity under visible light irradiation. Additionally, it is clear that the 3DOM N-TiO<sub>2</sub> shows much higher photodegradation efficiency than N-TiO<sub>2</sub> catalyst, which can be attributed to the unique 3DOM structure of the sample. It is well known that 3DOM materials have large pore volume, periodicity and tailored pore structure, as well as exhibit multiple scattering and slow photo effects. Therefore, 3DOM structure not only can provide more surface active sites for the adsorption of pollution molecules but also have the advantages for improving mass transfer and increasing the path length of light, both of them contribute to the enhancement of light absorption and photoreaction efficiency<sup>11,12</sup>. Hence, we can attempt to conclude that the obtained 3DOM N doped TiO<sub>2</sub> catalysts show an excellent photocatalytic activity under visible-light irradiation owing to the synergistic effect of their special 3DOM structure, large pore volume, high crystallization degree, N doping system and higher charges separation.

In the meanwhile, the stability and reusability of the 3DOM N-TiO<sub>2</sub> catalyst was also tested by the photodegradation of RhB under visible light irradiation. As shown in Fig. 12, after three runs of photodegradation of RhB, the N-TiO<sub>2</sub> with 3DOM structures still shows high photocatalytic activity, and the photodegradation efficiency reached to 68.04% within 120 min visible light illumination, which is slightly higher than that of the first round photodegradation. The recycling test clearly reveals that the as-prepared catalysts are quite stable and possess high recyclability, may be have excellent application potential in water treatment.

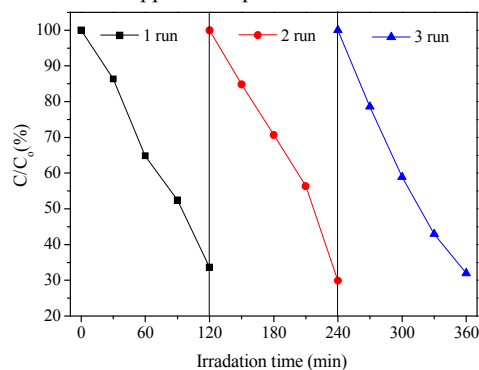


Fig. 12 Recycling tests of RhB photodegradation over 3DOM N-TiO<sub>2</sub> within 120 min visible-light irradiation.

Based on the above analysis and our previous reports<sup>24</sup>, a possible mechanism of visible light driven photocatalytic activity over 3DOM N-TiO<sub>2</sub> was proposed and schematically illustrated in Fig. 13. As is known to all, the doping of nitrogen in the lattice of TiO<sub>2</sub> could modify the electronic band structure of TiO<sub>2</sub>, resulting in the formation of substitutional electronic states (N 2p band) above the top of the O 2p valence band, which therefore narrows the band gap of TiO<sub>2</sub> and induces optical absorption into the visible light region<sup>24</sup>.

Hence, with the illumination of visible light, the 3DOM N-TiO<sub>2</sub> sample can be easily excited and produced a large number of electron-hole pairs on the N 2p midgap, and then the photogenerated electrons are quickly transferred to the CB of anatase TiO<sub>2</sub> away from the N 2p midgap state while leave holes in the original N 2p midgap and eventually disperse to the surface of macroporous walls of the 3DOM photocatalysts. This process of charge transfer inhibits the recombination of electrons and holes and provides the opportunities for these charges to participate in the oxidation-reduction reactions. On the one hand, it is well known that the presence of a 3DOM network within the N doped TiO<sub>2</sub> sample could provide vast reactive sites and allow better diffusion of reactants (-OH, oxygen, RhB), meanwhile, the interconnected macroporous network might facilitate the mass transfer and lead to easy accessibility of active sites for the reactant molecules<sup>44</sup>. In the photoreaction, the electrons existed on the wall surface would be collected by the adsorbed O<sub>2</sub> to generate superoxide radical (O<sub>2</sub><sup>-•</sup>) and hydrogen peroxide radical (H<sub>2</sub>O<sub>2</sub>). Alternatively, the two active species might produce chemical reaction each other to generate hydroxyl radicals (•OH) for the purpose of reacting with RhB molecules and oxidizing water molecules. On the other hand, the holes not only could directly oxidize RhB molecules but also could react with -OH adsorbed on surface of the photocatalyst to generate hydroxyl radical (•OH)<sup>45</sup>. Therefore, it can be concluded that the 3DOM N-TiO<sub>2</sub> shows an excellent photocatalytic activity under visible-light irradiation owing to the synergistic effect of hydroxyl radical and holes.

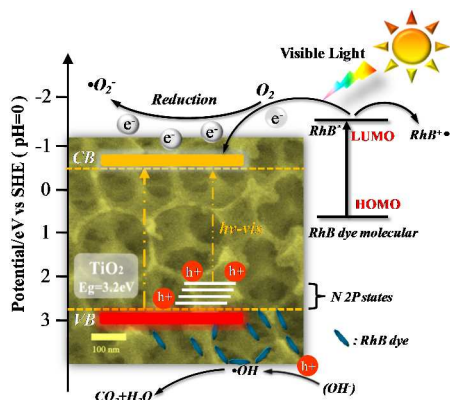


Fig. 13 Scheme illustrating the principle of charge-transfer and the photocatalytic processes on the interface of the 3DOM N-TiO<sub>2</sub> under visiblelight irradiation.

Moreover, except for the cooperative effect of the •OH and holes, RhB can be photosensitized and produce electrons under visible light illumination<sup>42</sup>, which again favors the enhancement of the photocatalytic activity. As shown in Fig. 13, the photogenerated electrons on the LUMO level of the photoexcited RhB dye can easily and rapidly transfer to the CB of TiO<sub>2</sub>. Meanwhile, due to the existence of superoxide radical (•O<sub>2</sub><sup>-</sup>), RhB dye could be transformed into the cationic dye radical (RhB<sup>•+</sup>), which can be degraded into intermediate products and eventually decomposed to CO<sub>2</sub> and H<sub>2</sub>O. However, as the superoxide radical (•O<sub>2</sub><sup>-</sup>) could react with hydrogen peroxide (H<sub>2</sub>O<sub>2</sub>), the photosensitization of RhB described above was not the key factor for the enhanced photocatalytic activity<sup>14</sup>.

## Conclusions

N doped TiO<sub>2</sub> with three-dimensional ordered macroporous structure was successfully fabricated by one-step colloidal crystal template method using the ethanediamine as the nitrogen resource. The results show that the N species have been doped in TiO<sub>2</sub> lattice, and the formation of N 2p intermediate energy levels in the band gap leads to enhanced visible light absorption of 3DOM N-TiO<sub>2</sub>. Besides, the obtained sample shows excellent photocatalytic activity for the degradation of RhB and the generation of H<sub>2</sub> under visible light irradiation, which can be attributed to the synergetic effect of uniform three-dimensional ordered macroporous structure, N doping and stronger visible light absorption.

## Acknowledgements

This work was financially supported by the National Natural Science Foundation of China (Grant No. 21303130), the Fundamental Research Funds for the Central Universities and Natural Science Basic Research Plan in Shaanxi Province of China (Grant No. 2014JQ2066).

## Notes and references

<sup>a</sup> Department of Chemical Engineering, School of Chemical Engineering and Technology, Xi'an Jiaotong University, Xi'an, 710049, China. Fax: (+86) 29-8266-3189; E-mail: guidongyang@mail.xjtu.edu.cn

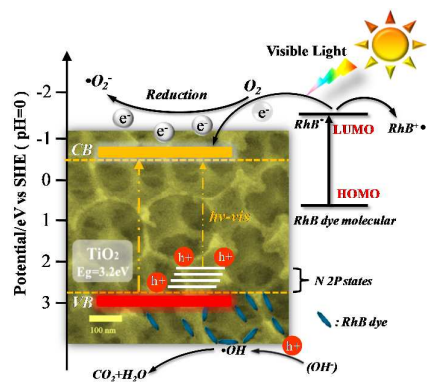
<sup>b</sup> Department of Applied Chemistry, School of Science, Xi'an Jiaotong University, Xi'an, 710049, China.

<sup>c</sup> Electronic Materials Research Laboratory, Key Laboratory of the Ministry of Education, Center for Dielectric Research, Xi'an Jiaotong University, Xi'an 710049, China.

<sup>d</sup> Department of Environmental Science & Engineering, Xi'an Jiaotong University, Xi'an 710049, China.

- Z. Wang, N. S. Ergang, M. A. Al-Daous, A. Stein, *Chem. Mater.* 2005, **17**, 6805-6813.
- F. Cheng, Z. Tao, J. Liang, J. Chen, *Chem. Mater.* 2008, **20**, 667-681.
- K. T. Lee, J. Cho, *Nano Today*, 2011, **6**, 28-41.
- R. C. Schroden, C. F. Blanford, B. J. Melde, B. J. S. Johnson, A. Stein, *Chem. Mater.* 2001, **13**, 1074-1081.
- S. Madhavi, C. Ferraris, T. White, *J. Solid State Chem.*, 2006, **179**, 866-872.
- J. E. G. J. Wijnhoven, W. L. Vos, *Science*, 1998, **281**, 802-804.
- Y. Chen, Y. Zhu, Z. Chen, *Thin Solid Films*, 2013, **539**, 122-126.
- M. Sawangphruk, J. Limtrakul, *Mater. Lett.*, 2012, **68**, 230-233.
- Y. Wei, Z. Zhao, T. Li, J. Liu, A. Duan, G. Jiang, *Appl. Catal. B: Environ.*, 2014, **146**, 57-70.
- S. Chai, G. Zhao, Y. Wang, Y.-N. Zhang, Y. Wang, Y. Jin, X. Huang, *Appl. Catal. B: Environ.*, 2014, **147**, 275-286.
- M. Wu, Y. Li, Z. Deng, B.-L. Su, *ChemSusChem*, 2011, **4**, 1481-1488.
- J. I. L. Chen, G. von Freymann, S. Y. Choi, V. Kitaev, G. A. Ozin, *Adv. Mater.*, 2006, **18**, 1915-1919.
- G. Yang, B. Yang, T. Xiao, Z. Yan, *Appl. Surf. Sci.*, 2013, **283**, 402-410.

- 14 C. Xue, T. Wang, G. Yang, B. Yang, S. Ding, *J. Mater. Chem. A*, 2014, **2**, 7674-7679.
- 15 Y. Cao, T. He, L. Zhao, E. Wang, W. Yang, Y. Cao, *J. Phys. Chem. C*, 2009, **113**, 18121-18124.
- 16 G. Yang, Z. Yan, T. Xiao, *Appl. Surf. Sci.*, 2012, **258**, 4016-4022.
- 17 G. Yang, T. Wang, B. Yang, Z. Yan, S. Ding, *Appl. Surf. Sci.*, 2013, **287**, 135-142.
- 18 S. C. Hayden, N. K. Allam, M. A. El-Sayed, *J. Am. Chem. Soc.*, 2010, **132**, 14406-14408.
- 19 G. Yang, Z. Yan, T. Xiao, *Appl. Surf. Sci.*, 2012, **258**, 8704-8712.
- 20 Y. Liu, L. Zhou, Y. Hu, C. Guo, H. Qian, F. Zhang and X. W. Lou, *J. Mater. Chem.*, 2011, **21**, 18359-18364.
- 21 Y. Ao, J. Xu, S. Zhang, D. Fu, *Appl. Surf. Sci.*, 2010, **256**, 2754-2758.
- 22 J. Geng, D. Yang, J. Zhu, D. Chen, Z. Jiang, *Mater. Res. Bull.*, 2009, **44**, 146-150.
- 23 M. M. Joshi, N. K. Labhsetwar, P. A. Mangrulkar, S. N. Tijare, S. P. Kamle, S. S. Rayalu, *Appl. Catal. A*, 2009, **357**, 26-33.
- 24 G. Yang, Z. Jiang, H. Shi, T. Xiao, Z. Yan, *J. Mater. Chem.*, 2010, **20**, 5301-5309.
- 25 R. C. Schroden, M. Al-Daous, C. F. Blanford, A. Stein, *Chem. Mater.* 2002, **14**, 3305-3315.
- 26 Q. Li, J. K. Shang, *J. Am. Ceram. Soc.*, 2008, **91**, 660-663.
- 27 Y. Ao, J. Xu, D. Fu, C. Yuan, *J. Hazard. Mater.*, 2009, **167**, 413-417.
- 28 K. L. Yeung, S. T. Yau, A. J. Maira, J. M. Coronado, J. Soria, P. L. Yue, *J. Catal.*, 2003, **219**, 107-116.
- 29 Y. Huo, Y. Jin, J. Zhu, H. Li, *Appl. Catal. B*, 2009, **89**, 543-550.
- 30 J. Zhang, Y. Wang, J. Jin, J. Zhang, Z. Lin, F. Huang, J. Yu, *ACS Appl. Mater. Interfaces*, 2013, **5**, 10317-10324.
- 31 B. Brunauer, L. S. Deming, W. S. Deming, E. J. Teller, *Am. Chem. Soc.*, 1940, **62**, 1723.
- 32 J. Yu, L. Qi, *J. Hazard. Mater.* 2009, **169**, 221-227.
- 33 P. G. O'Brien, N. P. Kherani, S. Zukotynski, G. A. Ozin, E. Vekris, N. Tetreault, A. Chutinan, S. John, A. Mihi, H. Miguez, *Adv. Mater.*, 2007, **19**, 4177-4182.
- 34 Y. C. Zhang, J. Li, H. Y. Hu, *Appl. Catal., B*, 2012, **123**, 20.
- 35 K. Yu, S. Yang, H. He, C. Sun, C. Gu, Y. Ju, *J. Phys. Chem. A*, 2009, **113**, 10024-10032.
- 36 J. Wang, W. Zhu, Y. Zhang, S. Liu, *J. Phys. Chem. C*, 2007, **111**, 1010.
- 37 Y. Sheng, Y. Xu, D. Jiang, L. Liang, D. Wu, Y. Sun, *Int. J. photoenergy*, 2008, **2008**, 1
- 38 S. Hoang, S. Guo, N. T. Hahn, A. J. Bard, C. B. Mullins, *Nano Lett.*, 2012, **12**, 26-32.
- 39 X. Chen, C. Burda, *J. Am. Chem. Soc.*, 2008, **130**, 5018-5019.
- 40 A. Fujishima, X. T. Zhang, D. A. Tryk, *Surf. Sci. Rep.*, 2008, **63**, 515-582.
- 41 B. Liu, L.-M. Liu, X.-F. Lang, H.-Y. Wang, X. W. Lou, E. S. Aydil, *Energy Environ. Sci.*, DOI: 10.1039/C4EE00472H (2014).
- 42 T. Wang, G. Yang, J. Liu, B. Yang, S. Ding, Z. Yan, T. Xiao, *Appl. Surf. Sci.*, 2014, **311**, 314-323.
- 43 X. Xu, G. Yang, J. Liang, S. Ding, C. Tang, H. Yang, W. Yan, G. Yang, D. Yang, *J. Mater. Chem. A*, 2014, **2**, 116-122.
- 44 Y. Dong, Y. Wang, T. Cai, L. Kou, G. Yang, Z. Yan, *Ceram. Int.* 2014, **40**, 11213-11219.
- 45 Y. Wang, W. Yang, L. Zhang, Y. Hu, X. W. Lou, *Nanoscale*, 2013, **5**, 10864-10867.



N doped TiO<sub>2</sub> with three-dimensional ordered macroporous structure was fabricated by one-step colloidal crystal template method, which showed excellent photocatalytic activity for the degradation of dye and the generation of H<sub>2</sub> under visible light irradiation